

Inflationary vs. Reionization Features from *Planck* 2015 Data

Georges Obied,¹ Cora Dvorkin,¹ Chen Heinrich,² Wayne Hu,³ and V. Miranda⁴

¹*Harvard University, Department of Physics,
Cambridge, MA 02138, USA*

²*Jet Propulsion Laboratory, California Institute of Technology, Pasadena California 91109*

³*Kavli Institute for Cosmological Physics, Department of Astronomy & Astrophysics,
Enrico Fermi Institute, University of Chicago, Chicago, IL 60637*

⁴*Center for Particle Cosmology, Department of Physics and Astronomy,
University of Pennsylvania, Philadelphia, Pennsylvania 19104, USA*

Features during inflation and reionization leave corresponding features in the temperature and polarization power spectra that could potentially explain anomalies in the *Planck* 2015 data but require a joint analysis to disentangle. We study the interplay between these two effects using a model-independent parametrization of the inflationary power spectrum and the ionization history. Preference for a sharp suppression of large scale power is driven by a feature in the temperature power spectrum at multipoles $\ell \sim 20$, whereas preference for a component of high redshift ionization is driven by a sharp excess of polarization power at $\ell \sim 10$ when compared with the lowest multipoles. Marginalizing inflationary freedom does not weaken the preference for $z \gtrsim 10$ ionization, whereas marginalizing reionization freedom slightly enhances the preference for an inflationary feature but can also mask its direct signature in polarization. The inflation and reionization interpretation of these features makes predictions for the polarization spectrum which can be tested in future precision measurements especially at $10 \lesssim \ell \lesssim 40$.

I. INTRODUCTION

Measurements of the anisotropies of the cosmic microwave background (CMB) are entering the era wherein both the temperature and polarization spectra will be determined to near cosmic variance precision across the linear regime. Indeed CMB measurements have already helped establish the cosmological constant cold dark matter (Λ CDM) model with nearly scale invariant inflationary initial conditions as the standard cosmological model. Its concordance with other high precision cosmological probes such as Type IA supernovae, baryon acoustic oscillations and Big Bang Nucleosynthesis lends strong support for the basic framework of Λ CDM.

Nonetheless, there are a few well-known tensions and glitches in the CMB power spectra that seem to hint at deviations from the standard cosmological model. With improvement in CMB polarization data in particular, we can search for matching features and consistency tests for potential physical explanations of these features.

In this work we focus on the large angle features in temperature and polarization power spectra and test their potential explanation from corresponding features from inflation and reionization. The standard Λ CDM cosmology assumes that the reionization of hydrogen atoms in our universe happened suddenly in redshift, but reionization cannot occur instantaneously and with multiple sources of ionizing radiation could in principle be quite extended in redshift [1–3]. Features in the *Planck* 2015 polarization data indeed allow and even favor a component of ionization at $z \gtrsim 10$ when the complete information out to a limiting redshift is included in a reionization model independent approach [4, 5] (see also [6]).

Incorrect assumptions about the ionization history can bias not only the Thomson total optical depth [7–9] but

also inferences on parameters not directly related to the physics of reionization such as the sum of the neutrino masses [10, 11] and tests of the inflationary consistency relation [12]. Optical depth constraints when combined with measurements of the heights of the acoustic peaks also impact the gravitational lensing interpretation of oscillatory residuals in the *Planck* temperature power spectrum from Λ CDM at high multipole [13, 14].

Moreover, if reionization indeed is more complicated than a steplike transition it can in principle impact the interpretation of the $\ell \sim 20 - 40$ features in the temperature power spectrum as well as its confirmation in polarization spectra if the range of features overlap [15]. The interpretation of these features affects the calibration of the physical size of the sound horizon and hence the inference of the Hubble constant from the acoustic peaks [13, 14] which is in tension with the local distance ladder measurements (e.g. [16]).

These features could potentially indicate transient violations of slow-roll conditions during the inflationary epoch [17–21]. Most attempts to model such behavior have been constructed *a posteriori* which makes a statistical interpretation of the significance of deviations from Λ CDM difficult to interpret. Model-independent approaches typically find lower significance per parameter [22–29] making the search for matching features in polarization and their disentanglement from reionization even more important [15, 29, 30].

It is also natural to ask whether these or other known features in the temperature power spectrum influence the reionization interpretation of polarization measurements. For example a suppression of large scale power in the inflationary spectrum would require a higher optical depth during reionization to produce the same polarization spectrum. Conversely, the measurement of finite

polarization power at the lowest multipoles requires the existence of horizon scale inflationary fluctuations even beyond the Λ CDM model [31].

In this work we combine the model independent approaches to reionization [4, 32] and inflation [14] to address these issues. We can then draw conclusions about inflationary features while marginalizing the impact of ionization history assumptions and vice versa. We also examine the predictions each make for future polarization measurements which could confirm their physical interpretation.

This paper is organized as follows: we describe the data and models considered in this work in Sec. II, analyze the implications of temperature and polarization features for inflation and reionization in Sec. III, and discuss our results in Sec. IV. In Appendix A, we illustrate the ability of future cosmic variance limited polarization measurements to improve reionization constraints.

II. DATA AND MODELS

In the analysis presented in this work, we use the *Planck* 2015 CMB power spectra as provided in the publicly available likelihood functions. Since reionization constraints and their impact on the large scale curvature power spectrum rely mainly on polarization spectra, we use the low multipole ($2 \leq \ell \leq 29$) lowTEB and the high multipole ($\ell \geq 30$) joint TTTEEE plik likelihood. Parameter inference in each of the models is carried out with a modified version of the Boltzmann solver CAMB [33, 34] linked to the Markov Chain Monte Carlo public code COSMOMC [35, 36].

The baseline case is the standard Λ CDM model with parameters $\Omega_b h^2$ for the baryon density, $\Omega_c h^2$ for the cold dark matter density, θ_{MC} for the effective angular scale of the sound horizon, and τ for the total Thomson optical depth. In this baseline model, the inflationary initial conditions are parametrized by the amplitude A_s and tilt n_s of the curvature power spectrum $\Delta_{\mathcal{R}}^2 = A_s(k/k_0)^{n_s-1}$ where the pivot scale is $k_0 = 0.08 \text{ Mpc}^{-1}$. Hydrogen reionization is taken to be a steplike transition and parametrized by the total optical depth τ through reionization (see Ref. [4] for details).

We investigate models which provide more freedom in the reionization and inflationary histories. For the former, we focus on the average ionization fraction $x_e(z)$, as appropriate for large angle power spectra. Here we allow arbitrary variations around a fiducial model of the ionization fraction [32]:

$$x_e(z) = x_e^{\text{fid}}(z) + \sum_a t_a S_a(z), \quad (1)$$

where $S_a(z)$ are the principal components of the cosmic variance limited EE Fisher matrix for x_e perturbations between $z_{\min} = 6$ and z_{\max} as constructed in Ref. [37], t_a are their amplitudes and $x_e^{\text{fid}}(z)$ is the fiducial model. For details of the fiducial model, see Ref. [4] and note

Model	Added Param.	$-2\Delta \ln \mathcal{L}$
Λ CDM	τ	0.0
Rei	t_a	5.7
Ifn	τ, p_i	17.9
Ifn+Rei	t_a, p_i	22.3

TABLE I. Models, the parameters they add to the fundamental set $\{\ln A_s, n_s, \theta_{MC}, \Omega_b h^2, \Omega_c h^2\}$, and their maximum likelihoods relative to Λ CDM. In Λ CDM and Ifn, reionization is parametrized by the total optical depth τ of a steplike transition. The 20 parameters p_i are spline basis coefficients that generalize the inflationary tilt on large scales [14]. The 5 parameters t_a are the amplitudes of ionization history principal components [4].

that hydrogen is fully ionized for $z < z_{\min}$ whereas it follows the recombination ionization fraction for $z > z_{\max}$ and is constant in between. We choose $z_{\max} = 30$ since the *Planck* data do not significantly prefer any ionization above this redshift [5]. We retain the first 5 principal components since they suffice to describe any ionization history in this range to the cosmic variance limit.

For arbitrary t_a , the ionization fraction described by Eq. (1) can exceed the physical bounds imposed by zero and full ionization. We follow Refs. [4, 37] in placing necessary but not sufficient priors on t_a to limit unphysical behavior. We cannot impose strictly sufficient priors using only 5 principal components because the omitted components, although irrelevant for the observable power spectrum, do affect the physicality of the ionization history. These omitted components tend to give oscillatory and not cumulative contributions (see Fig. 15) and so we can better identify model-independent constraints on the ionization history through the cumulative optical depth

$$\tau(z, z_{\max}) = n_H \sigma_T \int_z^{z_{\max}} dz \frac{x_e(z)(1+z)^2}{H(z)}, \quad (2)$$

where n_H is the number density of hydrogen today and σ_T is the Thomson cross section. Of course when using these PC constraints for testing specific physical models, physical priors are automatically established and t_a constraints can be applied directly [2–4].

On the other hand, for the inflationary curvature spectrum we parameterize the local slope of the power spectrum in a manner consistent with inflationary dynamics using the Generalized Slow-Roll (GSR) formalism [27, 28, 38, 39],

$$\frac{d \ln \Delta_{\mathcal{R}}^2}{d \ln k} \rightarrow -G' \equiv (n_s - 1) - \delta G', \quad (3)$$

with

$$\delta G'(\ln s) = \sum_i p_i B_i(\ln s). \quad (4)$$

Deviations from a constant slope are characterized by amplitudes p_i and a spline basis $B_i(\ln s)$ where $s \equiv \int d \ln a \, c_s(aH)^{-1}$ is the inflaton sound horizon. Unlike a direct parametrization of $\Delta_{\mathcal{R}}^2$, this technique has the

benefit of automatically enforcing the inflationary requirement that the sharper the temporal feature, the more it rings to higher k , which is important for modeling sharp features in the TT spectrum. We choose 20 logarithmically spaced spline knots in the range $200 < s/\text{Mpc} < 20000$ in order to parameterize large-scale deviations from power-law initial conditions. We restrict the range of G' so as to bound power spectrum corrections that violate the linearity of Eq. (3) by taking the second order parameter $|I_1| < 1/\sqrt{2}$, as discussed in Ref. [28].

In order to eliminate correlations between the amplitudes p_i and identify the strongest constraints, we then define the inflationary principal component amplitudes $m_a \equiv \sum_i p_i V_{ia}$ where V_{ia} is an orthonormal matrix of eigenvectors of the covariance matrix between the parameters p_i obtained from the MCMC chains. We choose to report the 3 m_a coefficients with the smallest errors. Note that unlike reionization PCs, which are precomputed for completeness from a cosmic variance limited measurement of the fiducial model, the inflationary PCs are defined with respect to the *Planck* data. When adding reionization freedom to inflationary freedom, we keep the principal component basis V_{ia} fixed to those determined for the steplike reionization transition in order to enable direct comparisons between the two cases. For visualization purposes we construct the 3 PC filtered deviations from power law spectra

$$\delta G'(\ln s_i) = \sum_{a=1}^3 m_a V_{ia} \quad (5)$$

and spline interpolate between the i samples. Likewise we construct the 3 PC filtered version of the curvature power spectrum $\Delta_{\mathcal{R}}^2$ from $\delta G'$. This visualization highlights the impact of the most significant aspects of the deviations but should not be interpreted as direct constraints on $\Delta_{\mathcal{R}}^2$ (see Fig. 8).

In summary, the models used in this paper correspond to replacing the optical depth τ of a steplike ionization history with the reionization parameters t_a and/or adding the inflationary parameters p_i to the fundamental ΛCDM parameters $\{\Omega_b h^2, \Omega_c h^2, \theta_{\text{MC}}, \ln A_s, n_s\}$ (see Tab. I). We assume flat priors in each of these parameters out to ranges that are either uninformative compared with the data or limited by the above-mentioned restrictions on reionization and inflation. Note that for reionization, a flat prior in t_a does not correspond to a flat prior in the total τ due to the enhanced freedom to vary the ionization history at high redshift [40]. Any preference for higher τ should be accompanied by a better fit to the data or interpreted in a model context with priors on physical parameters (e.g. [3, 5]).

The maximum likelihood (ML) model of each parametrization is shown along with the data in Fig. 1. In the lower panels we scale the residuals against the

ΛCDM ML model to the cosmic variance per ℓ mode

$$\sigma_\ell = \begin{cases} \sqrt{\frac{2}{2\ell+1}} C_\ell^{TT}, & TT; \\ \sqrt{\frac{1}{2\ell+1}} \sqrt{C_\ell^{TT} C_\ell^{EE} + (C_\ell^{TE})^2}, & TE; \\ \sqrt{\frac{2}{2\ell+1}} C_\ell^{EE}, & EE, \end{cases} \quad (6)$$

evaluated using the fiducial reionization model. We use this model for convenience since the ΛCDM steplike reionization history produces an EE spectrum whose cosmic variance is too far below the *Planck* noise variance at $10 \lesssim \ell \lesssim 30$ to be practical. Note that the data and models in Fig. 1 have been rescaled by 1/4 for TE and 1/20 for EE to fit on the same scale as the near cosmic variance limited TT measurements. This scaling also highlights that there is significant opportunity for improvement in polarization measurements which can be used to test the interpretation of both reionization and inflation features in the future.

The likelihood improvements of these models over ΛCDM is given in Tab. I. While these improvements do not justify the introduction of 5 ionization parameters and 20 new inflationary parameters, our parameterization aims for completeness in the characterization of power spectra features. These model-independent constraints can then be used to test specific models with fewer parameters or find matching features within and between the temperature and polarization spectra that could reveal their physical origin.

For reionization, the 5 parameters currently represent one new aspect of the model class, the ability to have a significant component of the total optical depth at $z > 10$ [5], whereas for inflation the 3 PC compression highlights the coherent features rather than the statistical fluctuations of the low- ℓ power spectra. Notice also that the improvements from reionization and inflation parameters are nearly additive, indicating that they are controlled by almost independent aspects of the data.

Indeed the reionization and inflation parameters fit mostly separate features in the various power spectra at low- ℓ as shown in Fig. 1. The well known deficit of power in TT around $\ell \sim 20$ mainly drives the inflationary degrees of freedom whereas the excess in EE around $\ell \sim 10$ drives preferences for high redshift ionization. The TE power spectrum naturally combines features in both T and E due to their correlation. We explore next the interplay between these features in the data and constraints on reionization and inflation.

III. REIONIZATION AND INFLATION

In this section, we discuss the implications of polarization and temperature power spectra features on separate and joint constraints of reionization history and inflation.

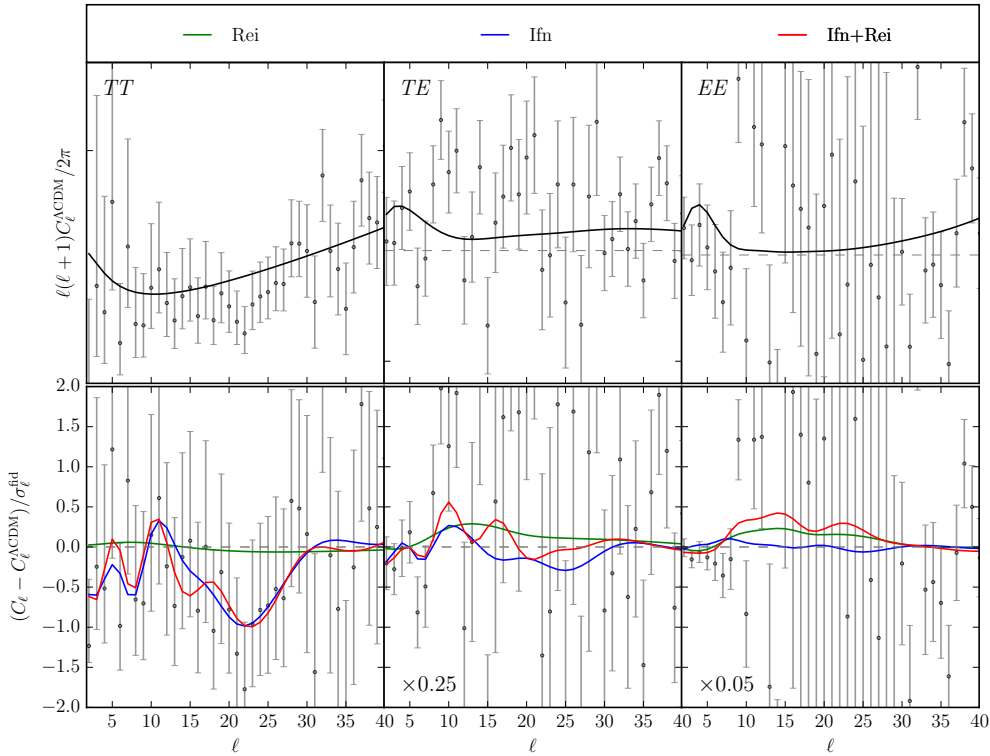


FIG. 1. *Planck* power spectrum data vs. the best fit models within the various classes. Top panel: baseline Λ CDM model with power law inflationary curvature spectrum and steplike reionization. Bottom panel: residuals with respect to Λ CDM in the data and the models with additional freedom in reionization (Rei), inflation (Inf), and both (Inf+Rei). Residuals are scaled to the cosmic variance per ℓ of the fiducial reionization model as well as a further scaling of 0.25 (*TE*) and 0.05 (*EE*) to fit to the *TT* scale. Features in *TT* drive inflationary constraints, especially around $\ell \sim 20$ and those in *EE* drive reionization constraints, especially around $\ell \sim 10$.

A. Polarization Features and Reionization History

CMB polarization is particularly sensitive to the ionization history since it is generated only when a quadrupole temperature anisotropy is scattered by free electrons. During reionization, the *EE*-mode polarization spectrum gains a feature at scales that roughly correspond to the horizon size at the respective redshift where these quadrupoles form from streaming radiation. Measurements of this feature provides coarse-grained constraints on the ionization history, and in particular, on the amount of high vs. low z optical depth.

On the other hand, the usual imposition of a steplike reionization requires the optical depth to mainly come from low redshifts. In the Rei model we relax this assumption by adding the 5 PCs t_a . In the Rei+Ifn model, we test the robustness of reionization constraints to features in the curvature power spectrum.

Ref. [4] found that once the steplike imposition is relaxed with reionization PCs, the *Planck* 2015 data not only allows but also is better fit by a high $z \gtrsim 10$ component with a 95% CL preference for finite contributions at $z \gtrsim 15$ (see also [5, 6]). In Fig. 1 we see that this preference is driven by a sharp increase in *EE* power at

$\ell = 9$ with several points that average high thereafter. As pointed out in Ref. [41], $\ell = 9$ is anomalously high at 2.7σ if a steplike reionization is assumed. In addition $\ell = 9$ is slightly low in *TT* even though the two should be positively correlated. In the steplike model, power at these multipoles cannot be raised without violating the constraints from the very low power at $2 \leq \ell \leq 8$. In fact, in the steplike model, the best fit is a compromise between these very low and very high points as shown in Fig. 1. By allowing low ionization at low redshift and high ionization at high redshift relative to a step, the reionization PCs can better thread through these constraints. These models make very different and testable predictions for the polarization spectrum at $10 \lesssim \ell \lesssim 40$.

In Fig. 2 we show the posterior distribution of C_ℓ^{EE} from the various cases analyzed in this paper. The ability to raise *EE* power at $9 \leq \ell \leq 15$ requires reionization freedom as can be seen from the similarity of Rei and Inf+Rei and conversely the lack of power in both Λ CDM and Inf constraints. Inflationary degrees of freedom produce a matching set of features between *EE* and *TT* once projection effects are taken into account. Therefore they cannot alone be responsible for a feature in *EE* that is not present in *TT*.

When added to reionization features, inflationary fea-

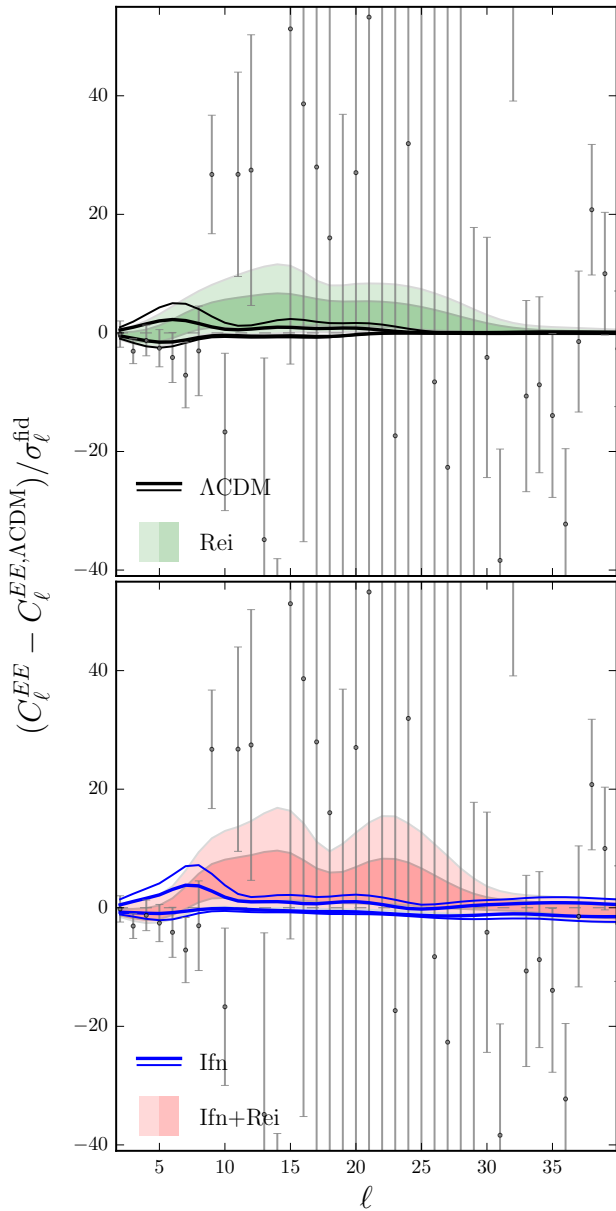


FIG. 2. EE power spectrum constraints for the various model classes (68% and 95% CL). Constraints are driven by the high power at $\ell = 9$ and the several following multipoles which favor high redshift ionization in the Rei and Inf+Rei classes and cannot be fit with Inf alone. Models and data are plotted with respect to the best fit ΛCDM model as in Fig. 1.

tures can marginally help sharpen the rise in power at $\ell \sim 9$ due to a matching rise at $\ell \sim 11$ in TT . Note also that cosmic variance does not correlate statistical fluctuations at different multipoles between the two spectra despite the TE correlation, whereas physical effects require an offset in multipoles due to projection effects [15]. Cosmic variance does make the significance of this joint feature weak. With Ifn+Rei, the data favor slightly less ionization at $z \lesssim 15$ and allow more at $z \gtrsim 15$ which then leads to more freedom to raise EE in the $20 \lesssim \ell \lesssim 25$ regime where a signal is yet to be measured. This free-

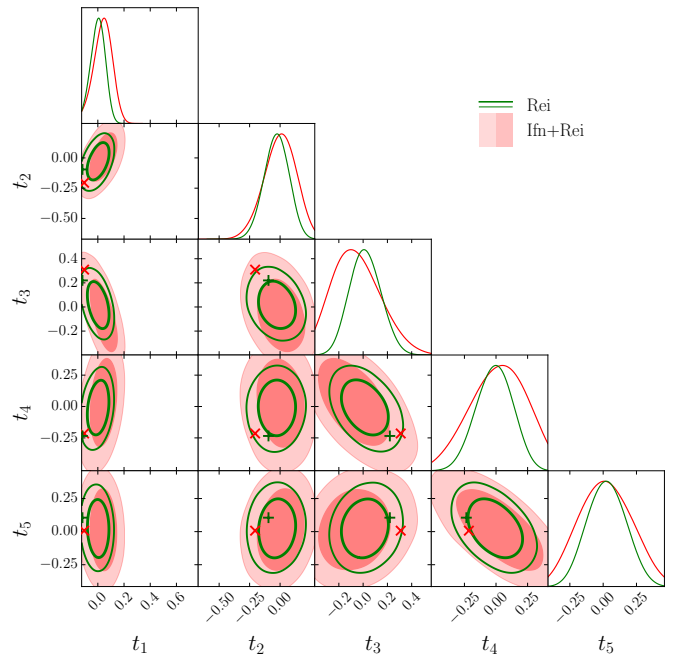


FIG. 3. Reionization PC constraints with (red) and without (green) inflationary p_i parameters marginalized (68% and 95% CL). The red \times and green $+$ indicate the best fit steplike reionization history in the respective classes and lies outside the preferred regime, especially in t_1 and t_2 .

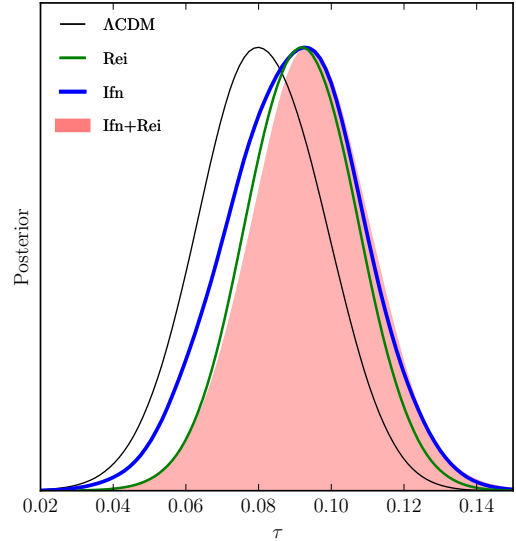


FIG. 4. Total optical depth τ constraints in the various model classes.

dom can fully mask features that come from inflation alone shown in Fig. 2 which are due to the TT feature in this regime unless they can be excluded by measurements in other ℓ ranges [15] or in the context of specific physical reionization models.

We can also see these effects in the constraints on the

reionization PCs t_a and their implications for the cumulative optical depth in Figs. 3 and 5. Constraints on t_a broaden moderately when marginalizing the additional p_i inflationary degrees of freedom. The boundaries of the panels represent the weak physicality constraint on the ionization history described in the previous section. Without the inflationary degrees of freedom, the priors just clip the allowed region for negative values of t_1 , corresponding to forbidding negative ionization at $z \gtrsim 15$. The fact that the posterior peaks away from this boundary indicates that the data in fact favor some ionization at $z \gtrsim 15$. This is borne out by the cumulative τ constraints where there is a 95% CL preference for finite contributions there. Were it not for the priors, the impact of marginalizing p_i on t_4 and t_5 would be more apparent as these parameters are currently better constrained by the reionization Doppler effect on the temperature power spectrum at intermediate multipoles below the first acoustic peak than by the polarization power spectrum at low multipoles.

With inflationary degrees of freedom, physicality bounds also clip positive fluctuations in t_2 and negative fluctuations in t_3 which correspond to forbidding negative ionization at $z \lesssim 15$. In this case, models with essentially no ionization at $6 \lesssim z \lesssim 15$ are allowed. In fact the weak physicality priors still allow some negative ionization as discussed above. This can be seen in Fig. 5 where, within the 95% CL bounds, the cumulative optical depth is allowed to be non-monotonic with a peak between $10 \lesssim z \lesssim 15$. These reionization constraints for Rei+Ifn therefore err on the conservative side, especially in allowing additional excess EE power at $20 \lesssim \ell \lesssim 25$ over Rei.

Nonetheless, in the other direction, the 95% CL preference for finite contributions to τ at $z \gtrsim 15$ remains robust to inflationary features. This corresponds to the fact that inflationary freedom alone cannot substantially raise the EE power at $\ell \geq 9$ without changing the ionization history or violating TT constraints. Correspondingly in Fig. 3 the best fit steplike reionization model with (\times) and without (+) marginalizing inflationary parameters lies in the disfavored region especially in the $t_1 - t_2$ plane.

The $z = 0$ endpoint of the cumulative τ constraint is the total optical depth. In Fig. 4, we display its posterior in the various cases. In moving from Λ CDM to Ifn, τ increases but its errors remain similar. This is due to the fact that features in TT favor a net suppression of inflationary power so, in order to achieve the same EE power, we require higher τ . In the Rei model, τ increases and the width decreases. This reflects the ability to relax the tension that occurs in the steplike model between the low EE power at $\ell \leq 8$ and the high EE power at $\ell > 8$. Moving to the Ifn+Rei model has little impact on τ since the enhanced freedom to have ionization at $z \gtrsim 15$ is compensated by lower ionization at lower redshifts. Note also that the upper bounds on τ remain fairly robust in all of the extensions. The low power at

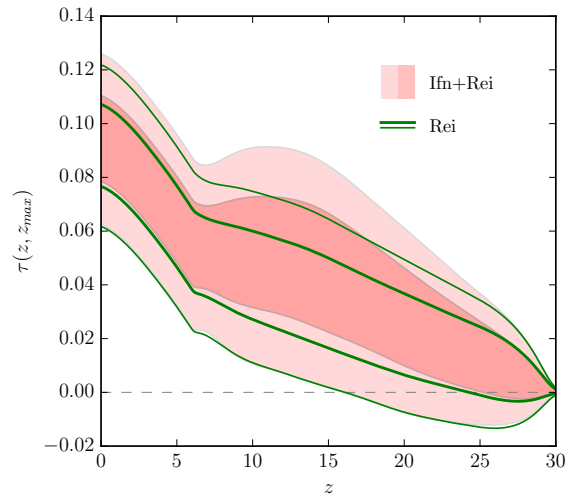


FIG. 5. Cumulative τ constraints (68% and 95% CL) for the Rei and Ifn+Rei class. In both cases there is a 95% CL preference for ionization at $z \gtrsim 15$ that cannot be accommodated with a steplike reionization history.

$\ell \leq 8$ constrains all models since high redshift ionization unavoidably contributes there as well due to projection effects (see Fig. 2 in Ref. [32]).

B. Temperature Features and Inflation History

The well known anomalies in the low multipole TT spectrum drive the constraints on features during inflation. In Fig. 6, we show the posterior constraints on the TT spectrum in the various model classes. In particular both Ifn and Ifn+Rei attempt to fit the suppression of power at $\ell \sim 20$ and a rise at $\ell \sim 11$ using the inflationary freedom, whereas neither Λ CDM nor Rei have the ability to do so. In these cases, the fiducial constant tilt model lies outside the 95% CL band from $20 \leq \ell \leq 25$.

As discussed in the previous section, the main impact of Rei freedom on the TT posterior is to slightly sharpen the rise at $\ell \sim 11$ due to the matching feature in polarization at $\ell \sim 9$ and the reduced necessity of excess curvature power to explain the EE spectrum at higher multipoles. While with inflationary parameters alone, Figs. 1 and 2 show that the TT feature at $\ell \sim 20$ is matched by an EE feature at $\ell \sim 25$ that is larger than the cosmic variance errors, they are much smaller than the *Planck* polarization errors there and can also be masked by reionization features.

The impact on the TE posterior from Ifn+Rei is stronger, as shown in Fig. 7. TE represents a combination of temperature and polarization features. Ifn alone produces similar features in TE as in TT . Rei alone produces a smooth excess in TE power at $\ell \sim 10 - 15$. The Ifn+Rei combination then contains elements of both showing a broad but pronounced feature at $\ell \sim 10 - 15$,

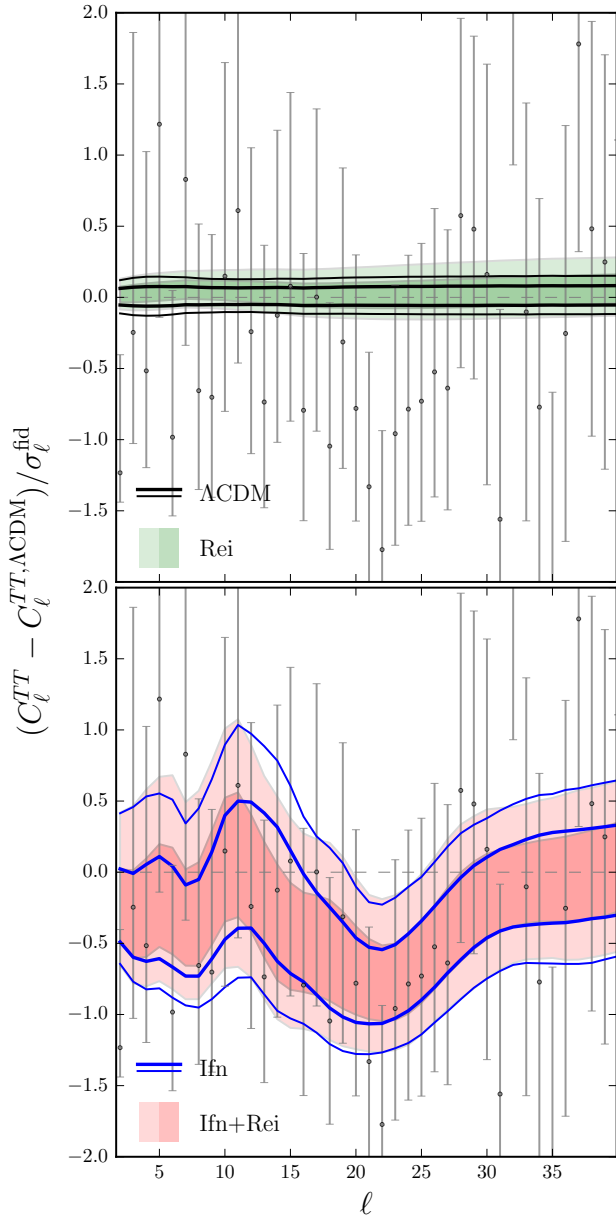


FIG. 6. TT power spectrum constraints for the various model classes (68% and 95% CL). Constraints are driven by the low power glitch around $\ell \sim 20$ which can be fit by models with inflationary freedom Inf and Inf+Rei but not by Rei alone. Models and data are plotted with respect to the best fit ΛCDM model as in Fig. 1

which best match the data.

Next we examine the implications of the *Planck* data for the inflationary parameters and initial conditions. In Fig. 8 shows the posterior constraints on the curvature power spectrum in the Inf case. Note that the TT feature at $\ell \sim 20$ corresponds to a dip in power at $k \approx 0.002 \text{ Mpc}^{-1}$ whereas the rise at $\ell \sim 11$ to the bump at $k \approx 0.001 \text{ Mpc}^{-1}$. By constructing the curvature power spectrum $\Delta_{\mathcal{R}}^2$ consistently from the inflationary source G' , we enforce the requirement that sharp temporal features during inflation lead to oscillatory features

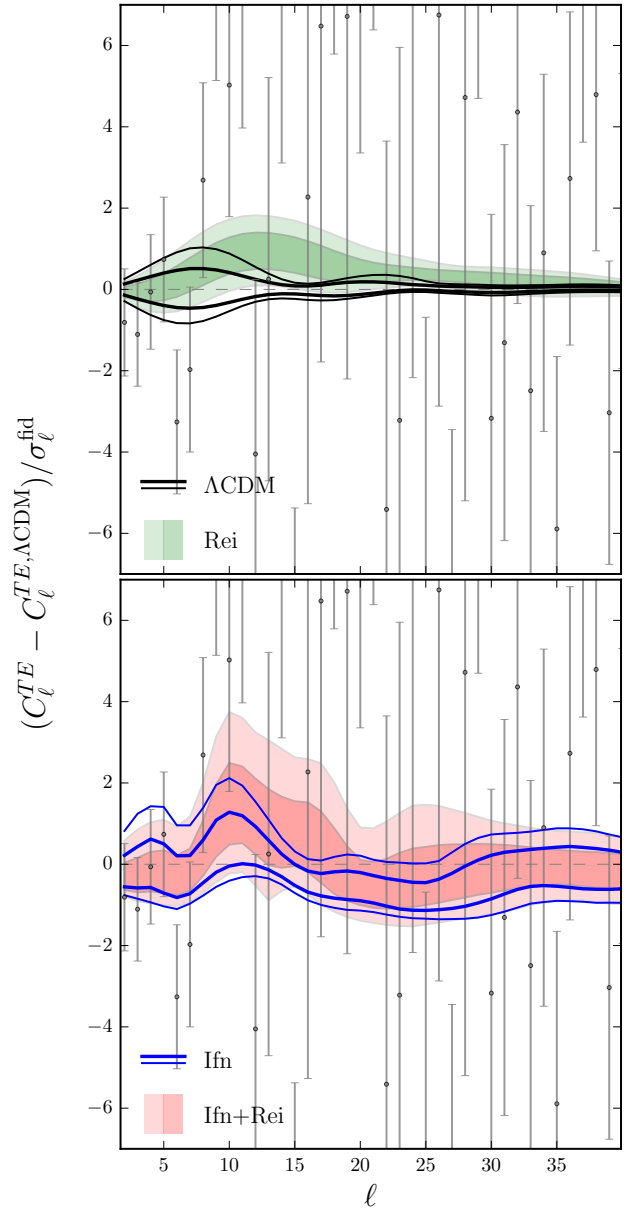


FIG. 7. TE power spectrum constraints for the various model classes (68% and 95% CL). Constraints follow the combined features of EE and TE shown in Figs. 2 and 6 allowing the Inf+Rei to best fit the $10 \lesssim \ell \lesssim 20$ regime. Models and data are plotted respect to the best fit ΛCDM model as in Fig. 1.

in the power spectrum.

On the other hand these oscillatory deviations also tend to fit out statistical fluctuations in the data. The inflationary PCs effectively filter out these low significance features. In Fig. 9, we show that inflationary principal component constraints under Inf. Notice that the slow roll prediction of $m_1 = m_2 = m_3 = 0$ lies outside the 95% CL region in the $m_2 - m_3$ plane. In Fig. 8 we show that this deviation is associated with a suppression in power at $k \lesssim 0.005 \text{ Mpc}^{-1}$.

These conclusions are largely robust to marginalizing reionization PCs in Inf+Rei. In fact, counterintuitively

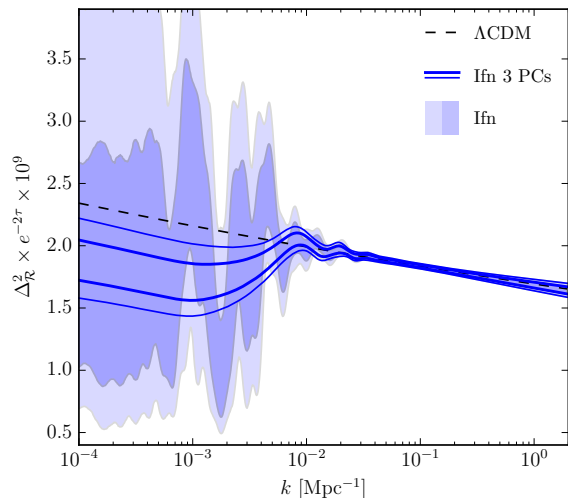


FIG. 8. Curvature power spectrum constraints for the Inf class (68% and 95% CL). The 20 parameters p_i fit fluctuations in the TT power spectrum shown in Fig. 6 and imply constraints on $\Delta_{\mathcal{R}}^2$ with the glitch at $\ell \sim 20$ corresponding to a dip at $k \sim 0.002$ Mpc $^{-1}$. The 3 PCs m_a filter out low significance features leaving a preference for less low k power than can be accommodated by slow-roll inflation.

all three PC components deviate slightly more from zero in Fig. 9 once reionization is marginalized, with little enhancement of their errors. In Fig. 10 we show that correspondingly the suppression of power at $k \lesssim 0.005$ Mpc $^{-1}$ is actually sharper once reionization is marginalized. The localization is even more apparent in the impact of the 3 inflationary PCs on $\delta G'$ shown in Fig. 11. Again, the suppression at large scales becomes slightly more rather than less significant when reionization is marginalized.

The reason for the enhancement of the inflationary feature by reionization can be understood mainly as the indirect effect of the higher total optical depth τ favored in the Inf+Rei case shown in Fig. 4. A larger τ lowers the acoustic peaks relative to the low- ℓ temperature power spectrum and therefore requires a larger suppression of low to high k from inflation to achieve the same TT spectrum. This larger suppression comes from both a slightly larger tilt ($n_s = 0.962 \pm 0.005$ for Inf and $n_s = 0.964 \pm 0.005$ for Inf+Rei) and a larger feature from the inflationary principal components.

These effects, however, are relatively minor so that the main conclusion is that the preference for an inflationary feature to explain the deficit of TT power at $\ell \sim 20$ remains even when all possible reionization histories between $6 \leq z \leq 30$ are marginalized with the reionization PCs.

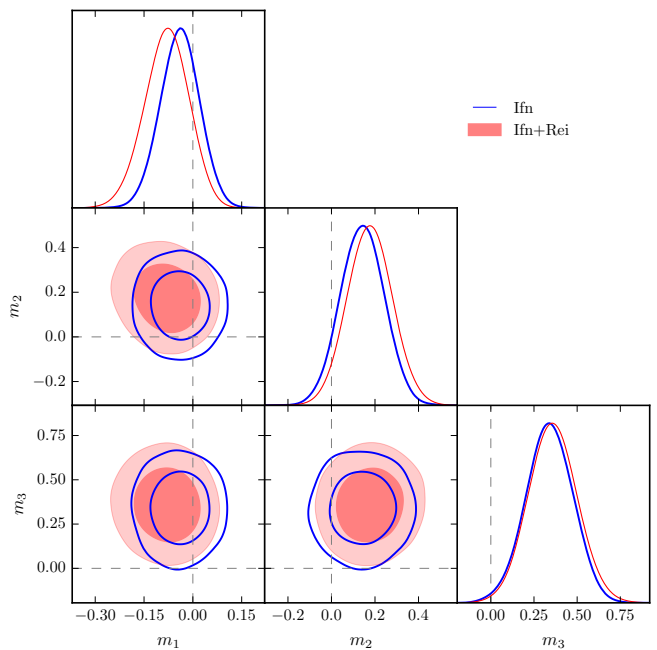


FIG. 9. Inflation 3 PC constraints (68% and 95% CL). The preference for deviations from power law inflationary conditions (dashed lines) remains and marginally increases once reionization parameters are marginalized in Inf+Rei.

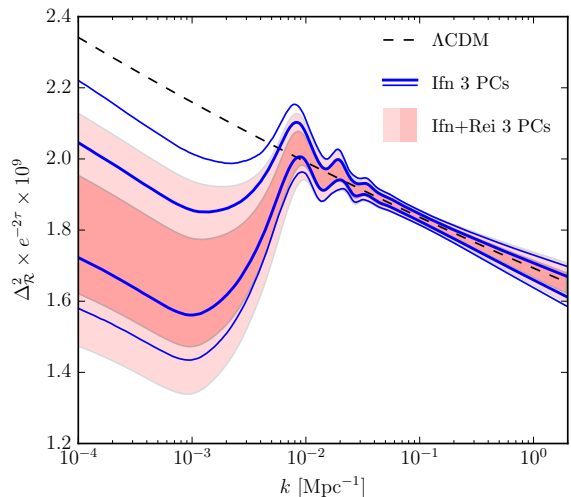


FIG. 10. Inflation 3 PC impact on the curvature power spectrum in Inf+Rei compared with Inf (68% and 95% CL). Marginalizing reionization parameters under Inf+Rei causes the net reduction of low k power to become larger to compensate for the larger total optical depth τ .

IV. DISCUSSION AND CONCLUSION

The low order multipoles of the CMB temperature and polarization spectra show anomalous features that could be explained by corresponding features during inflation and reionization. To the extent that these features over-

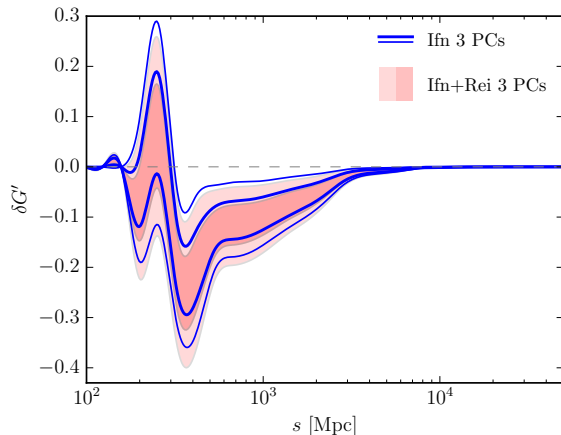


FIG. 11. Inflation 3 PC impact on $\delta G'$, the source of deviations from constant tilt, (68% and 95% CL). The feature at $\ell \sim 20$ in TT produces a similar localization of a sharp feature during inflation when the sound horizon was $s \sim 300$ Mpc. Marginalizing reionization parameters in Inf+Rei makes the decrement slightly larger.

lap, a joint analysis of inflation and reionization could reveal degeneracies between the two or favor one type over the other.

We find that in the *Planck* 2015 data the temperature and polarization features instead favor both inflation and reionization features with little interference between the two. More specifically, residuals in the *Planck* EE power spectrum taken with respect to the best fit Λ CDM model show an excess in power around $\ell \sim 10$ with noise dominated measurements at $\ell \sim 20$, while the TT power spectrum shows a suppression in power at $\ell \sim 20$ with no significant enhancement at $\ell \sim 10$. It is thus not possible to have a model where inflation alone accounts for the $\ell \sim 10$ feature nor is it possible for reionization to create a large temperature feature at $\ell \sim 20$.

Beyond a steplike reionization history, high redshift reionization at $z \gtrsim 10$ can better account for the high EE power, especially at $\ell = 9$, while simultaneously maintaining low power at $\ell < 9$ that is required by the data. Marginalizing inflationary parameters does not reduce the significance of lower limits to the cumulative optical depth at $z \gtrsim 10$.

Likewise, an inflationary feature that transiently violates the slow-roll approximation is compatible with the sharp suppression at $\ell \sim 20$. The two sets of features do interfere in the sense that high redshift reionization could potentially mask the matching EE feature predicted by an inflationary explanation for the TT feature. However, counterintuitively, marginalizing over reionization PCs makes the inflationary feature slightly more rather than less significant. The larger optical depth associated with high redshift ionization requires more suppression of large scale power relative to the acoustic peaks.

Physically, this interpretation of the two observed set

of features implies two independent events in the cosmic history, with those in the TT power spectrum relating to effects of slow-roll violation during inflation while the ones in the EE spectrum being the result of early reionization. Currently the significance of these features is fairly low, with high redshift reionization favored at $2\Delta \ln \mathcal{L} \sim 6$ and inflationary features separately at $2\Delta \ln \mathcal{L} \sim 18$ but with 20 extra parameters. The 3 best constrained combinations of the 20 parameters are responsible for sharply suppressing large scale inflationary power while the rest optimize the fine scale features to fluctuations in the TT spectrum.

In the future, polarization measurements at $10 \lesssim \ell \lesssim 40$ could potentially improve by more than an order of magnitude before hitting the cosmic variance limit. With such improvements, the inflation and reionization explanations of current measurements can be more definitively tested and disentangled. In particular, as explicitly shown in Appendix A, if the preferred ionization history lies in the center of the allowed region in Fig. 2, i.e. the Rei and Ifn+Rei contours, it could be distinguished from a Λ CDM model.

Appendix A: Cosmic Variance Limited E-mode Measurements

In this Appendix, we demonstrate the ability of future CV-limited measurements of the EE polarization spectrum to distinguish models with extended reionization from a steplike ionization history. For simplicity, we focus on the Rei case, where the EE spectrum cannot be altered by changes in the inflationary PCs. We note that, since $\Delta C_\ell \propto C_\ell$ for a CV-limited measurement, future C_ℓ constraints depend on the specific model within the Rei class assumed for the projected measurements.

1. Models and CV-limited Data

A comparison of C_ℓ^{EE} posteriors from Λ CDM versus the Rei model (shown in the top panel of Fig. 2) indicates that additional data in the multipole range $\ell = 14 - 30$ may substantially improve reionization constraints and more definitively test the steplike “Tanh” reionization history. In order to quantitatively study the effects of new data, we post-process our Rei chains assuming that

Future Data	Label
None	Current
Λ CDM bf $\ell = 14 - 30$	CV _{Tanh}
Rei bf $\ell = 14 - 30$	CV _{PC}

TABLE II. A summary of the post-processed Rei chains, the new data added and our labelling conventions. For example, “ Λ CDM bf $\ell = 14 - 30$ ” means that CV-limited measurements for C_ℓ^{EE} from $\ell = 14 - 30$ identical in value to the *Planck* 2015 Λ CDM best fit were added to *Planck* 2015 EE data.

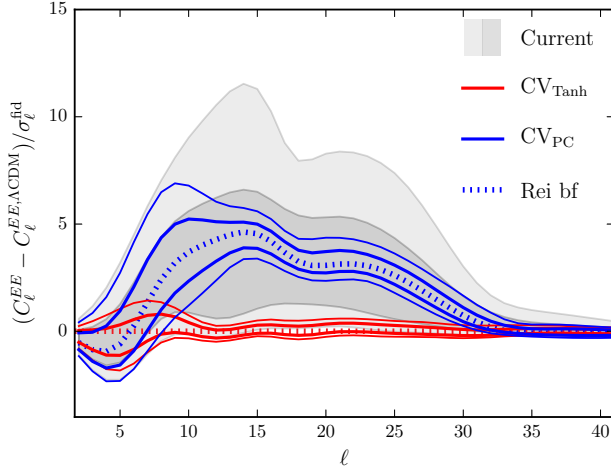


FIG. 12. EE power spectrum constraints for additional future CV-limited EE identical to the best fit Tanh model to current data (red) or PC extended model (blue) compared to current Rei constraints (gray) (68% and 95% CL). The *Planck* 2015 Rei best fit (blue dotted) is in good agreement with the CV_{PC} means. Note that the Tanh bf model is the horizontal line at zero.

	Current	CV_{Tanh}	CV_{PC}
t_1	0.002 ± 0.053	-0.090 ± 0.013	0.027 ± 0.013
t_2	-0.029 ± 0.101	-0.081 ± 0.040	0.007 ± 0.063
t_3	0.018 ± 0.127	0.114 ± 0.064	0.015 ± 0.076
t_4	-0.012 ± 0.143	-0.114 ± 0.098	0.045 ± 0.110
t_5	0.026 ± 0.142	0.070 ± 0.133	0.023 ± 0.132

TABLE III. Mean and standard deviation of the amplitudes of the reionization PCs. Note that the CV_{PC} case has larger errors compared to CV_{Tanh} due to the larger values of CIEE as simulated future data.

future measurements return values of C_ℓ^{EE} that are identical to either the *Planck* 2015 Λ CDM (Tanh) or Rei best fit. Importance sampling is performed by reweighting all samples by a factor of the new likelihood $\mathcal{L}_{\text{future}}$ given by:

$$-2 \ln \mathcal{L}_{\text{future}} = \sum_{\ell} (2\ell + 1) \left(\frac{\hat{C}_\ell^{EE}}{C_\ell^{EE}} - \ln \frac{\hat{C}_\ell^{EE}}{C_\ell^{EE}} - 1 \right),$$

where \hat{C}_ℓ^{EE} is the future measurement, C_ℓ^{EE} is the model and the sum runs over values of ℓ where we assume new data is available. For the ℓ -range of new data we take $\ell = 14 - 30$ which gives insight into how much we can eventually learn about reionization from a CV-limited EE spectrum. Different assumptions on future data and the models are summarized in Table II. The current data itself in this range provide negligible constraints in comparison for any of these choices and so this procedure does not significantly double count information.

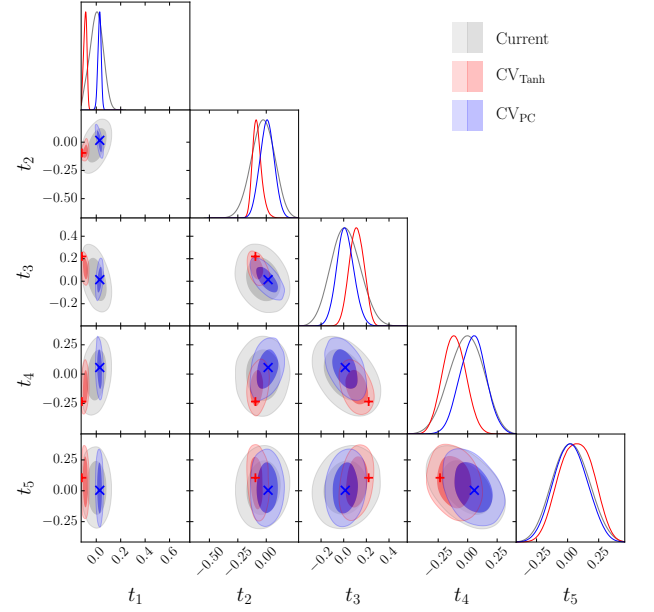


FIG. 13. Reionization PC constraints with current data combined with future cosmic variance limited EE data in the range $\ell = 14 - 30$ as in Fig. 12. The red \times and blue $+$ indicate these assumed models. In the Λ CDM case, the combined data posteriors are not centered on the assumed model for the future data since the current data alone (gray) disfavor the Tanh reionization history.

2. Improved Parameter Estimates

Assuming additional CV limited data severely limits the allowed C_ℓ^{EE} model space compared with current constraints. This is illustrated in Fig. 12 which shows that the two models are clearly \rightarrow easily distinguishable with a significance greater than 95% CL over the whole multipole range $10 \leq \ell \leq 30$. As anticipated, the extended reionization history model is very strongly disfavored for future data concordant with the Tanh model and vice versa.

A similar story is visible in t_a space (see Fig. 13) with $t_1 = -0.090 \pm 0.013$ for CV_{Tanh} and $t_1 = 0.027 \pm 0.013$ for CV_{PC} so that the means are separated by $\sim 9\sigma$. This figure also illustrates the bias of current data against a steplike reionization history. Note that the crosses ‘ \times ’ and plusses ‘ $+$ ’ show the true t_a values for the future data in each case. The constraints in the Λ CDM case are consistently displaced toward the Rei best fit points whereas the converse constraints are not. A summary of the means and standard deviations of the reionization parameters is shown in Table III.

Assuming a CV-limited measurement at a single EE multipole at for example $\ell = 14$ still yields a separation in t_1 sufficient to distinguish between a steplike and extended reionization models. For the CV_{Tanh} case, we have $t_1 = -0.072 \pm 0.022$ while for the CV_{PC} case, we have $t_1 = 0.031 \pm 0.023$ such that their means are separated by $\sim 4.5\sigma$.

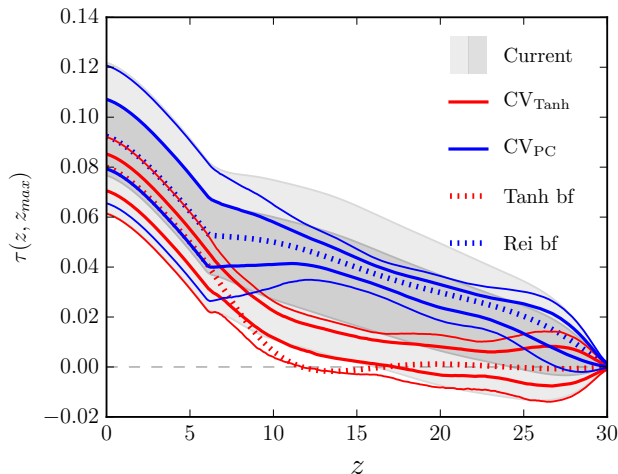


FIG. 14. Cumulative optical depth $\tau(z, z_{\max})$ constraints with future CV-limited EE data as in Fig. 12. For the Λ CDM case, the current data slightly biases the joint constraints toward high- z optical depth ($z \gtrsim 11$) compared with the steplike ionization history assumed for the additional data.

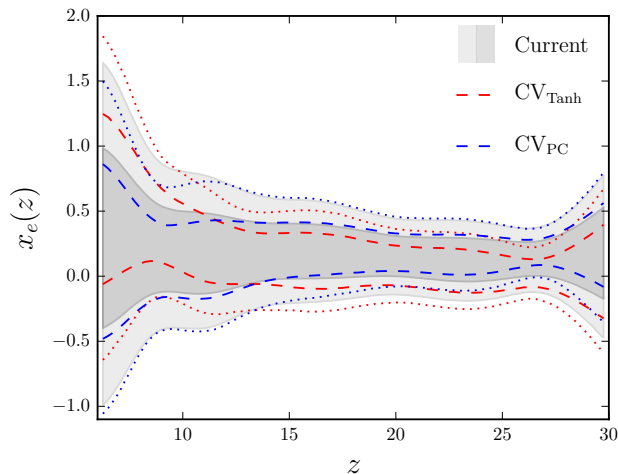


FIG. 15. Free electron fraction $x_e(z)$ constraints including future CV-limited EE data as in Fig. 12. Note that even simulated CV-limited EE data is not sufficient to constrain the ionization fraction despite improved cumulative optical depth constraints shown in Fig. 14.

3. Optical Depth from High Redshift

Improved constraints on t_a also imply improved constraints on $\tau(z, z_{\max})$. These are shown in Fig. 14. The two cases are distinguished at high statistical significance through the $z = 10 - 25$ range. Notably, assuming future data is CV_{Tanh} the constraints still allow for some contributions to $\tau(z, z_{\max})$ from $z \gtrsim 11$ as opposed to its assumed Tanh model. This reflects the fact that current data inherently prefers a non-zero contribution at these redshifts.

4. Reionization Fraction Constraints

Finally, for completeness we consider constraints on the free electron fraction $x_e(z)$ as derived from the 5 t_a constraints as shown in Fig. 15. As mentioned in the main text, this visualization of the constraints emphasizes the most poorly constrained parameters which allow high frequency oscillations in x_e . Even with CV-limited data, the improvement in t_4 and t_5 is not enough to make the reconstructed x_e a good representation of the constraints. In particular t_5 is mainly constrained by the Doppler contributions to the temperature power spectrum rather than polarization. This representation would give the misleading impression that the Tanh and PC models are indistinguishable despite the clear separation of the models in t_1 .

Moreover, had we included more than 5 t_a parameters, this representation would become even more misleading. Since the $x_e(z)$ reconstruction highlights the least constrained direction in t_a space, the contours would eventually reflect only the priors and not the data. This means that the CMB is not capable of constraining the ionization fraction at any one particular redshift despite good constraints on the cumulative $\tau(z, z_{\max})$ for all z moderately less than z_{\max} .

ACKNOWLEDGMENTS

GO and CD were supported by the Dean's Competitive Fund for Promising Scholarship at Harvard University. CH was supported by Jet Propulsion Laboratory, California Institute of Technology, under a contract with the National Aeronautics and Space Administration. WH was supported by U.S. Dept. of Energy contract DE-FG02-13ER41958, NASA ATP NNX15AK22G and the Simons Foundation. Computing resources were provided by the University of Chicago Research Computing Center through the Kavli Institute for Cosmological Physics at the University of Chicago.

-
- [1] R. Barkana and A. Loeb, *Phys. Rept.* **349**, 125 (2001), [arXiv:astro-ph/0010468 \[astro-ph\]](#).
 - [2] K. Ahn, I. T. Iliev, P. R. Shapiro, G. Mellema, J. Koda, and Y. Mao, *Astrophys. J.* **756**, L16 (2012), [arXiv:1206.5007 \[astro-ph.CO\]](#).
 - [3] V. Miranda, A. Lidz, C. H. Heinrich, and W. Hu, *Mon. Not. Roy. Astron. Soc.* **467**, 4050 (2017), [arXiv:1610.00691 \[astro-ph.CO\]](#).
 - [4] C. H. Heinrich, V. Miranda, and W. Hu, *Phys. Rev.* **D95**, 023513 (2017), [arXiv:1609.04788 \[astro-ph.CO\]](#).
 - [5] C. Heinrich and W. Hu, (2018), [arXiv:1802.00791 \[astro-ph.CO\]](#).
 - [6] D. K. Hazra and G. F. Smoot, *JCAP* **1711**, 028 (2017), [arXiv:1708.04913 \[astro-ph.CO\]](#).
 - [7] M. Kaplinghat, M. Chu, Z. Haiman, G. Holder, L. Knox, and C. Skordis, *Astrophys. J.* **583**, 24 (2003), [arXiv:astro-ph/0207591 \[astro-ph\]](#).
 - [8] G. Holder, Z. Haiman, M. Kaplinghat, and L. Knox, *Astrophys. J.* **595**, 13 (2003), [arXiv:astro-ph/0302404 \[astro-ph\]](#).
 - [9] L. P. L. Colombo, G. Bernardi, L. Casarini, R. Mainini, S. A. Bonometto, E. Carretti, and R. Fabbri, *Astron. Astrophys.* **435**, 413 (2005), [arXiv:astro-ph/0408022 \[astro-ph\]](#).
 - [10] K. M. Smith, W. Hu, and M. Kaplinghat, *Phys. Rev.* **D74**, 123002 (2006), [arXiv:astro-ph/0607315 \[astro-ph\]](#).
 - [11] R. Allison, P. Caucal, E. Calabrese, J. Dunkley, and T. Louis, *Phys. Rev.* **D92**, 123535 (2015), [arXiv:1509.07471 \[astro-ph.CO\]](#).
 - [12] M. J. Mortonson and W. Hu, *Phys. Rev.* **D77**, 043506 (2008), [arXiv:0710.4162 \[astro-ph\]](#).
 - [13] N. Aghanim *et al.* (Planck), (2016), [arXiv:1608.02487 \[astro-ph.CO\]](#).
 - [14] G. Obied, C. Dvorkin, C. Heinrich, W. Hu, and V. Miranda, *Phys. Rev.* **D96**, 083526 (2017), [arXiv:1706.09412 \[astro-ph.CO\]](#).
 - [15] M. J. Mortonson, C. Dvorkin, H. V. Peiris, and W. Hu, *Phys. Rev.* **D79**, 103519 (2009), [arXiv:0903.4920 \[astro-ph.CO\]](#).
 - [16] A. G. Riess, S. Casertano, W. Yuan, L. Macri, J. Anderson, J. W. Mackenty, J. B. Bowers, K. I. Clubb, A. V. Filippenko, D. O. Jones, and B. E. Tucker, *ArXiv e-prints* (2018), [arXiv:1801.01120 \[astro-ph.SR\]](#).
 - [17] A. A. Starobinsky, *JETP Lett.* **55**, 489 (1992), [*Pisma Zh. Eksp. Teor. Fiz.* 55,477(1992)].
 - [18] J. A. Adams, B. Cresswell, and R. Easther, *Phys. Rev.* **D64**, 123514 (2001), [arXiv:astro-ph/0102236 \[astro-ph\]](#).
 - [19] M. Joy, V. Sahni, and A. A. Starobinsky, *Phys. Rev.* **D77**, 023514 (2008), [arXiv:0711.1585 \[astro-ph\]](#).
 - [20] A. Ashoorioon and A. Krause, (2006), [arXiv:hep-th/0607001 \[hep-th\]](#).
 - [21] A. Ashoorioon, A. Krause, and K. Turzynski, *JCAP* **0902**, 014 (2009), [arXiv:0810.4660 \[hep-th\]](#).
 - [22] S. Hannestad, *JCAP* **0404**, 002 (2004), [arXiv:astro-ph/0311491 \[astro-ph\]](#).
 - [23] A. Shafieloo and T. Souradeep, *Phys. Rev.* **D70**, 043523 (2004), [arXiv:astro-ph/0312174 \[astro-ph\]](#).
 - [24] P. Mukherjee and Y. Wang, *The Astrophysical Journal* **599**, 1 (2003).
 - [25] A. Shafieloo, T. Souradeep, P. Manimaran, P. K. Panigrahi, and R. Rangarajan, *Phys. Rev.* **D75**, 123502 (2007), [arXiv:astro-ph/0611352 \[astro-ph\]](#).
 - [26] G. Nicholson and C. R. Contaldi, *Journal of Cosmology and Astroparticle Physics* **2009**, 011 (2009).
 - [27] C. Dvorkin and W. Hu, *Phys. Rev.* **D82**, 043513 (2010), [arXiv:1007.0215 \[astro-ph.CO\]](#).
 - [28] C. Dvorkin and W. Hu, *Phys. Rev.* **D84**, 063515 (2011), [arXiv:1106.4016 \[astro-ph.CO\]](#).
 - [29] V. Miranda, W. Hu, and C. Dvorkin, *Physical Review D* **91**, 063514 (2015).
 - [30] D. K. Hazra, D. Paoletti, M. Ballardini, F. Finelli, A. Shafieloo, G. F. Smoot, and A. A. Starobinsky, *JCAP* **1802**, 017 (2018), [arXiv:1710.01205 \[astro-ph.CO\]](#).
 - [31] M. J. Mortonson and W. Hu, *Phys. Rev.* **D80**, 027301 (2009), [arXiv:0906.3016 \[astro-ph.CO\]](#).
 - [32] W. Hu and G. P. Holder, *Phys. Rev.* **D68**, 023001 (2003), [arXiv:astro-ph/0303400 \[astro-ph\]](#).
 - [33] A. Lewis, A. Challinor, and A. Lasenby, *Astrophys. J.* **538**, 473 (2000), [arXiv:astro-ph/9911177 \[astro-ph\]](#).
 - [34] C. Howlett, A. Lewis, A. Hall, and A. Challinor, *JCAP* **1204**, 027 (2012), [arXiv:1201.3654 \[astro-ph.CO\]](#).
 - [35] A. Lewis and S. Bridle, *Phys. Rev.* **D66**, 103511 (2002), [arXiv:astro-ph/0205436 \[astro-ph\]](#).
 - [36] A. Lewis, *Phys. Rev.* **D87**, 103529 (2013), [arXiv:1304.4473 \[astro-ph.CO\]](#).
 - [37] M. J. Mortonson and W. Hu, *Astrophys. J.* **672**, 737 (2008), [arXiv:0705.1132 \[astro-ph\]](#).
 - [38] C. Dvorkin and W. Hu, *Phys. Rev.* **D81**, 023518 (2010), [arXiv:0910.2237 \[astro-ph.CO\]](#).
 - [39] W. Hu, *Phys. Rev.* **D84**, 027303 (2011), [arXiv:1104.4500 \[astro-ph.CO\]](#).
 - [40] M. J. Mortonson and W. Hu, *Astrophys. J.* **686**, L53 (2008), [arXiv:0804.2631 \[astro-ph\]](#).
 - [41] N. Aghanim *et al.* (Planck), *Astron. Astrophys.* **594**, A11 (2016), [arXiv:1507.02704 \[astro-ph.CO\]](#).